Atmospheric Conditions Leading to an Exceptional Fatal Flash Flood in the Negev Desert, Israel

Uri Dayan[1], Itamar M. Lensky[2], Baruch Ziv[3]

[1]Department of Geography, The Hebrew University of Jerusalem, Jerusalem, 9070227, Israel
5 [2]Department of Geography and Environment, Bar-Ilan University, Ramat-Gan, 5290002, Israel
[3]Department of Natural Sciences, The Open University of Israel, Raanana, Israel

Correspondence to: Itamar M. Lensky (itamar.lensky@biu.ac.il)

Abstract. The study deals with an intense rainstorm that hit the Middle East between 24 and 27 April 2018. The storm reached
10 its peak over Israel in April 26, when it produced a heavy flash flood that took the lives of ten people. The rainfall observed in
the southern Negev was comparable to the long-term annual rainfall there. The timing of the storm is also unique, at the end
of the rainy season, when rain is relatively rare and spotty. The study analyses the dynamic and thermodynamic conditions
that made this rainstorm one of the latest spring severe events in the region during the last 3 decades.

The synoptic background was an upper-level cut-off low that entered the region from west, along 30°N latitude, which is rather
15 exceptional for such systems in the late spring. While approaching the Levant, it slowed its movement from ~10 to <5 ms⁻¹.
On the day of maximum intensity, the radius of the cyclone shrank to 275 km. The effect of the small radius was estimated by
the measure of its curvature vorticity (MCV), which was the largest among the spring rainstorms during the latest 33 years.

The lower levels were dominated by a north-westerly wind that advected moist air from the Mediterranean inland. During the
approach of the storm, the atmosphere over Israel became unstable, with instability indices reaching values favourable for
20 thunderstorms (CAPE = 909 J Kg⁻¹, LI = -4.9 K, SI = -2.7 K and MKI = 30 K), and the precipitable water increased from 17
to 30 mm. The latter is explained here by a combined effect of the lower-level moisture advection and a mid-level band of
tropical moisture that entered Israel above it.

Three major rain centres were active during April 26, two of them were non-orographic, which is unusual for this type of
system. This is explained by the dominance of sub-synoptic features, found in the 0.25 resolution data of ERA5 that were used
25 to derive Omega and MKI maps. The build-up of static instability is explained by a -5 K temperature anomaly over the region,
caused by a northerly flow east of the blocking high over North Europe that transported cold air over the Mediterranean water.
The unique intensity of this storm is attributed to an amplification of a mid-latitude disturbance, which produced a cut-off low,
with its implied high relative vorticity, low upper-level temperatures and slow progression. All these, combined with the
contribution of several moisture sources, led to extreme dynamic and thermodynamic conditions favourable for this
30 exceptionally severe rainstorm.

1 Introduction

On April 26, 2018 an extremely intense rainstorm hit Israel. Ten people were killed by a raging flash flood in Tzafit creek, in the northeast of the Negev Desert (denoted in Fig. 1), that resulted from this storm. The rainfall depth during this storm exceeded 20 mm over ~ half of Israel, over most of which the monthly long-term mean does not exceed 10 mm.

35 Flash flood forecast and warning is a challenging task, in particular over remote arid areas, where meteorological radar coverage is sparse. Though flash flood warning has much improved in the last few decades, it is still the most weather-related fatal hazard globally (Montz et al. 2002), with 1,075 fatalities between 1996 and 2014 in the United States alone (Terti et al 2019). A significant part of flash flood victims is caused by incorrect assessment or misjudging of the risks of these rapidly evolving phenomena (Sharif et al. 2015; Becker et al. 2015; Diakakis et al. 2018).

40 The majority of the annual precipitation in Israel is associated with Mediterranean cyclones, while reaching its eastern part (i.e., Cyprus Lows, HMSO 1962; Saaroni et al. 2010; Zappa et al. 2015), two-thirds of which occur during December through February (Alpert et al. 2004; Ziv et al. 2006). The rest of the annual rainfall occurs in the transitional seasons and is contributed by precipitating tropical synoptic-scale systems and by Cyprus Lows. A significant part of them occur in the desert areas and are characterized as intensive rain events of small spatial extent and short duration, some of which produce flash floods

45 (Kahana et al. 2002; Dayan and Morin 2006, Greenbaum et al. 2010).

The aim of this study is to analyse the dynamic and thermodynamic conditions that turned this rainstorm into one of the latest spring severe events in the region during the last 33 years, and to explain its unique features, particularly the rain spatial distribution. The study concentrates on the Negev Desert, which is the southern half of Israel, located to the southeast of the Mediterranean.

50 The article is organized as follows: in the next section, we present the data and methods used to analyse the event. In section 3 we describe the event and identify the unique dynamic and thermodynamic conditions that lead to the severe convection, as well as the sources of moisture for the rain formation in this storm. Discussion and conclusions are presented in section 4.

2 Materials

The study area is the Negev Desert, covering the arid part of Israel, south of 31.2° N, and the Judean Desert (the latter is

55 denoted in Fig. 1), over which floods took place. The synoptic scale data, including satellite imagery, cover the entire Mediterranean Basin and South Europe.

The study covers a storm that influenced the study region between 24 and 27 April 2018, in particular to 26 April, when it reached its maximum intensity. This storm is compared to other 11 storms, spread over 28 days, in which discharge was observed over the study area, during April and May for the years 1986 – 2018, entitled hereafter the 'reference period'.

60 The rainfall analysis is based on the rain measuring network of the Israeli Meteorological Service (IMS Fig. 1) and the rain maps are taken from the IMS publication (Porat et al. 2018). The radar data is taken from the IMS radar, in terms of rain intensity (Marra and Morin 2015).
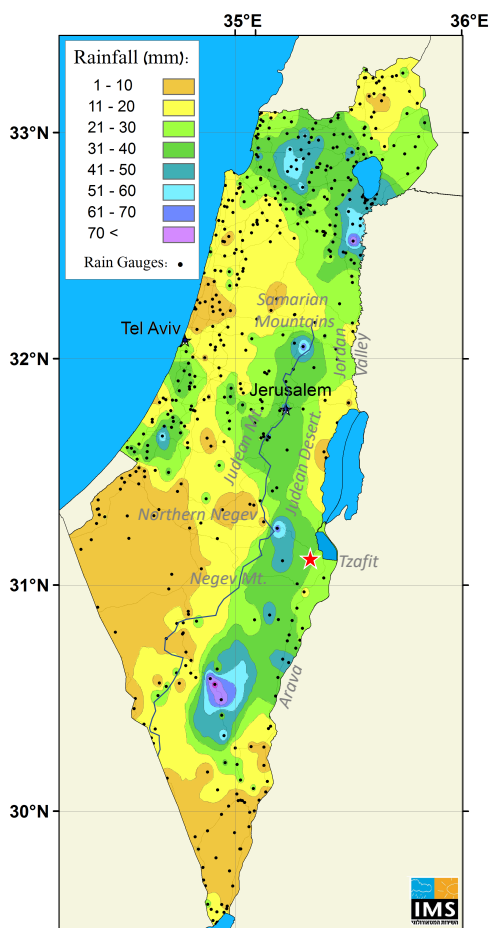
Figure 1: RADAR images of integrated rain over Israel (based on the Israeli Meteorological Service) for 25-27 April 2018. The black
65 **line indicates the water divide south of the Samarian Mountains.**

The data of floods during the reference period is based on the 11 maximum discharge storms measured over the Negev Desert,
the Dead Sea valley and the Arava by hydrometric stations of the Israeli Hydrological Service for April–May of the period
1986-2018.

The atmospheric processes responsible for flash flood-producing rainstorms act in concert at the synoptic and sub-synoptic
70 scales. The data for the synoptic maps, including sea level pressure (SLP) and upper-level fields, geopotential height (gph) and
vertical velocity (Omega), were taken from NCEP/NCAR reanalysis 1 database, with 2.5° x 2.5° spatial resolution (Kalnay et
al. 1996; Kistler et al. 2001). The analysis of the mesoscale features is based on ERA5 ECMWF reanalysis data base (C3S,
2017, https://cds.climate.copernicus.eu/cdsapp#!/dataset/reanalysis-era5-pressure-levels), with 0.25° x 0.25° resolution,
including wind field, relative vorticity, Omega and specific and relative humidity.

75 Several methodologies have been offered to quantify cyclone intensity and activity, Raible et al. (2007) for example, used the
mean gradient between the cyclone core and a radius of 1,000 km as a measure of cyclone intensity. Here the dynamic factors

addressed are vertical velocity and curvature vorticity. The latter is approximated by a 'measure of curvature vorticity' (MCV, hereafter). The MCV is calculated on the periphery of the upper-level (500 hPa) cyclones, based on the relation

$$\xi_c = V/R \ , \tag{1}$$

80 where ξ_c is curvature vorticity and V is the tangential wind speed. The cyclone radius, R, is that of the outer-most closed isohypse (when derived with 15 m intervals). The tangential wind speed was calculated using the geostrophic relation, i.e.,

$$V \cong g \times D/(R \times f) \ , \tag{2}$$

where g and f are gravitational acceleration and Coriolis parameter, respectively, and D is the depth of the cyclone. Inserting V from Eq. (2) in Eq. (1) yields:

85 $$MCV = g \times D/(R^2 \times f) \ . \tag{3}$$

Thermodynamic stability indices, based on the sounding data of Beit Dagan station, Israel (32.50° N, 34.81° E), were retrieved from the Department of Atmospheric Sciences, The University of Wyoming, at: http://weather.uwyo.edu/upperair/sounding.html. These are:

• Lifted Index (LI): Temperature difference between the environment and an air parcel lifted adiabatically at a given pressure
90 height in the troposphere (lowest layer where most weather occurs) of the atmosphere, usually 500 hPa (Galway 1956). Negative values indicate instability.

• The Showalter stability index (SI) is similar to the lifted index (LI), but while the LI starts with the mean of the lowest 100-hPa AGL layer, the SI uses a parcel lifted from 850 hPa to 500 hPa. At 500 hPa the parcel temperature is subtracted from the sounding temperature. More negative SSI values indicate greater instability (Showalter 1953).

95 • Convective Available Potential Energy (CAPE): The integrated energy excess of an air parcel lifted adiabatically with respect to its environmental temperature profile. (Moncrieff and Miller 1976). Values in the order of hundreds of J Kg^{-1} and more correspond to severe weather.

Maps of the Modified K-Index (MKI) were derived from the ERA5 ECMWF data, with a 0.25° resolution. The original K-Index (KI; Geer 1996), which combines instability and moisture availability, is used to predict severe thunderstorms in the
100 US. The modified version of Haratz et al. (2010), MKI, is the version adapted for the eastern Mediterranean:

$$MKI = (T_{500} - T_{850}) \times RH_{850,700} + Td_{850} - (T_{700} - Td_{700}) \ , \tag{4}$$

where T and Td are temperature and dew point, respectively, RH is relative humidity and the subscripts refer to the respective pressure level (hPa). The modification gives more weight to the relative humidity at the 850 and 700 hPa levels.

In addition, we also used Precipitable Water (PW), i.e., the depth of water in a column of the atmosphere, if all the water in that column were precipitated as rain (Liu, 1986).

Water vapor METEOSAT imageries were retrieved from Dundee Satellite Receiving Station, Dundee University, UK (http://www.sat.dundee.ac.uk/xrit/000.0E/MSG/2018/4/26/300/2018_4_26_300_MSG4_5_S1_grid.jpeg). Air back-trajectory for detecting moisture transport were retrieved from the site of NOAA HYSPLIT MODEL (Stein et al., 2015, https://www.ready.noaa.gov/HYSPLIT.php),

3 Analysis

Precipitation extremes and strong winds are usually induced by large-scale atmospheric circulation, namely low-pressure systems with large pressure gradients (Jacobeit et al. 2017; Knippertz 2018) therefore, this study was initiated by analyzing the synoptic circulation system with which this storm was associated. During 25–27 April 2018 the lower-levels were dominated by a cyclone, centred east of Israel (see Fig. 2). The implied winds were north-westerly, hence advecting moist air from the Mediterranean inland. This flow was perpendicular to the topographic upslope of the Judean Mountains and the northern Negev (see the water divide line denoted in Fig. 1), which activated convection within air parcels ascending there.

The rain in Israel started at April 25, reached its maximum intensity at April 26 and stopped at April 27 (IMS 2018). The spatial distribution of the rain deviated from the expected one in the sense that a considerable part of the major precipitative elements were observed over the downslopes of the mountain regions (Fig. 1). The maximum rainfall was obtained in the rain-shadow of the Negev Mountains, and the second most intense one was found in the Jordan valley, again, in the lee side of the Samarian Mountains. The dominance of convective over orographic elements suggests that sub-synoptic scale factors took place in this storm. This subject is elaborated below.

Two complementing factors contributed to the rain formation. One is dynamic, i.e., vertical ascent, associated with the cyclonic system described below (Sec. 3.2). The other is thermodynamic, which is composed of instability and moisture supply, described in Sec. 3.3.

3.1 Synoptic evolution

Prior to the storm, on April 24, 2018, the lower levels of the atmosphere were dominated by a Red Sea Trough (RST). The RST is a low-pressure system extending from south toward the Eastern Mediterranean (EM) and the Levant (Ashbel 1938; Kahana et al. 2002; Tsvieli and Zangvil 2005). The trough axis was located east of the Levant region, enclosing a shallow cyclone, with a central pressure of 1008 hPa, over north western Saudi Arabia (see Fig. 2a). This surface system transported warm and dry air from the east over the Levant. At the 500 hPa level, a closed cyclone was approaching the region from the central Mediterranean and slowed its progress during its arrival to the Egyptian coast, from ~9 ms^{-1} to ~4 ms^{-1} (see Fig. 3). There are difficulties in reaching a common view on the climatology of extra-tropical cyclone activities, e.g., size, lifetime and speed (Lionello et al. 2002; Ulbrich et al. 2009), which stem from different identification and tracking methods. However, it

135 should be noted that it is common to consider the average translation speed of extra-tropical cyclones is ~10 ms⁻¹ (Laurencin and Misra 2019).
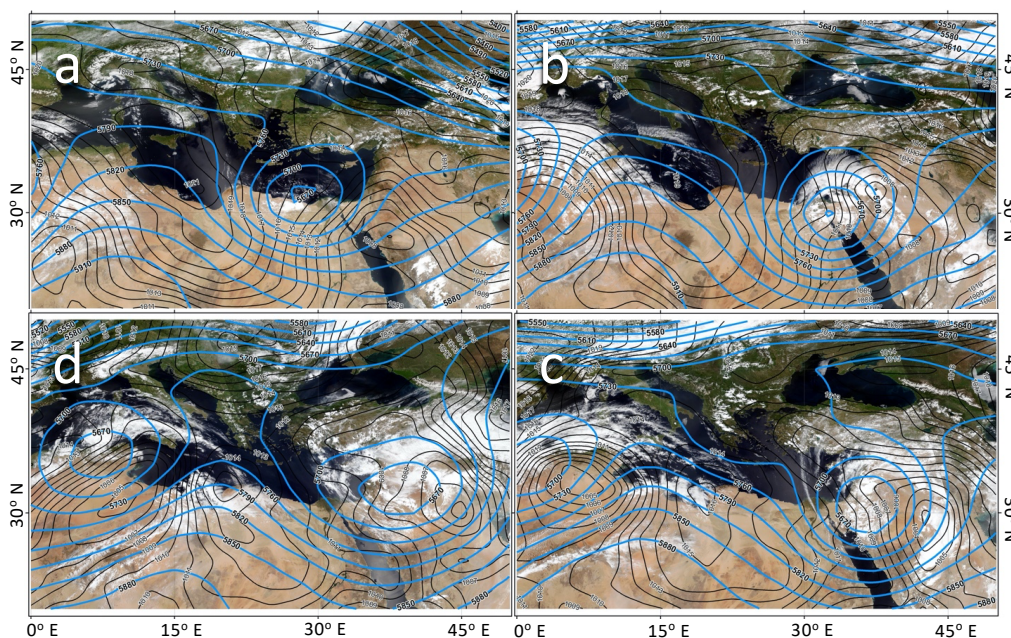
Figure 2: Geopotential height (GPH) at 500 hPa (m) and SLP (hPa) projected on MODIS imagery, in 24 h increments, for 24–27 April 2018, 12UTC (a–d, respectively).

140 The corresponding 300 hPa potential vorticity (PV) field shows a pronounced positive anomaly, with a maximum of 1.13 PVU (Fig. 4). Following Campa and Wernli (2012), this feature typifies mid-latitude cyclones. This is rather exceptional if one takes into account the timing of the late spring and the latitude along which the system moved (~30° N).

Upon initiation of the storm, on April 25, the 500 hPa cyclone continued to slow its eastward motion, with an average speed of 3.5 m sec⁻¹ and reached the Sinai Peninsula (Fig. 3). Concurrently, the surface cyclone that was imbedded in the RST

145 deepened (Fig. 2b) and moved northward. In the following day, on April 26, the storm attained its maximum intensity during noontime. The upper air cyclone in that day continued its slow eastward progression, which created a north-westerly flow across the entire atmospheric column over the EM (Fig. 2c). The weakening of the horizontal pressure gradient at the surface, in tandem with a flattening of the 500 hPa cyclone, on the following day (April 27, Fig. 2d), and its movement further eastward, lead to the cessation of the stormy weather over Israel.
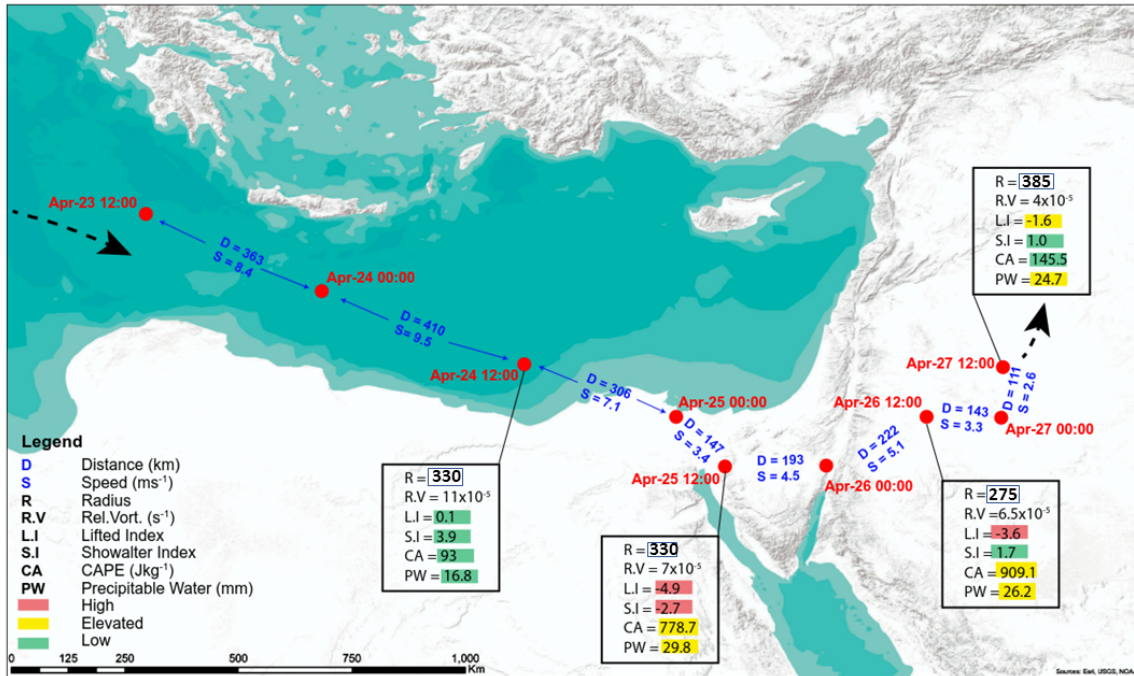
150

Figure 3: Course of the upper-level cyclone (500 hPa gph) during 24–27 April 2018, in 12 hours increments. The instantaneous speed (ms⁻¹) and distance (Km) spanned during each increment denoted by s and d, respectively. For each 24 hours increment, the radius of the upper-level low (Km), the maximum relative vorticity (s⁻¹), the precipitable water (mm) and 3 thermodynamic indices as calculated from the sounding of Beit Dagan are specified. "High", "Elevated" and "Low" values of the indices are highlighted in red, yellow and green, respectively.

155
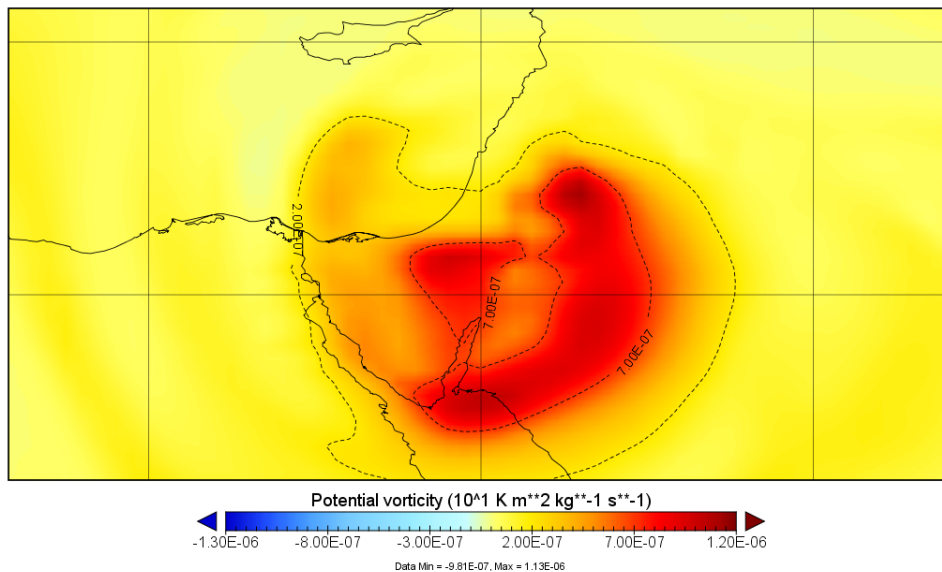
Figure 4: Potential Vorticity (K m² Kg⁻¹ s⁻¹) at 300 hPa for April 26 00 UTC, taken from ERA-5, with 0.25°×0.25° resolution. The major feature is a closed positive anomaly (with maximum of K m2 Kg⁻¹ s⁻¹), corresponding to a cut-off low, centred over north-western Saudi Arabia.

160   The identity of the upper-level cyclonic system as a cut-off low can be deduced from the isolated PV maximum (Hoskins et al. 1985), seen in April 26 00 UTC, 300 hPa map (Fig. 4). The slowing down of the upper-level cyclone while approaching the Egyptian coast is dynamically explainable in terms of point vortex interaction. This approach assumes that each point vortex induces a circular flow pattern that extends out of its core (e.g., Aref 1983). An example of interaction between two-point vortices is in the case of a dipole which consists of a blocking high located north of a cut-off low (Yamazaki and Itoh

165   2013). The interaction within such a dipole (presented schematically in Fig. 5) is expressed by easterly flow, induced by the blocking high, at the location of the cut-off low, and by easterly flow, induced by the cut-off low, over the blocking high.
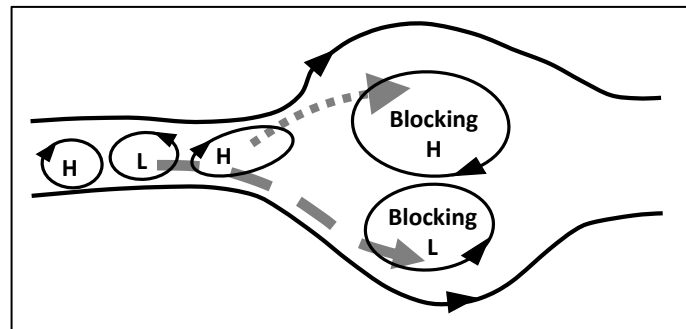
Figure 5: Conceptual diagram illustrating the dipole-type blocking pattern of a north-south blocking high and cutoff low (adapted from Yamazaki and Itoh, 2013).

170   Between April 24 and 25, a large anticyclone that covered Europe, split into two separated anticyclones (Figs. 6a and 6b). The eastern one, together with the cyclone over the south-eastern Mediterranean, formed a dipole-type structure system. The induced flow of each of the eastern anticyclonic and the cyclonic vortices slowed down the eastward propagation of each other against the westerly background flow. It should be noted that the deceleration of a cyclonic system is expected to further enhance its induced dynamic effects, i.e., divergence and vertical ascent (Palmen and Newton 1969; Ziv and Paldor 1999).
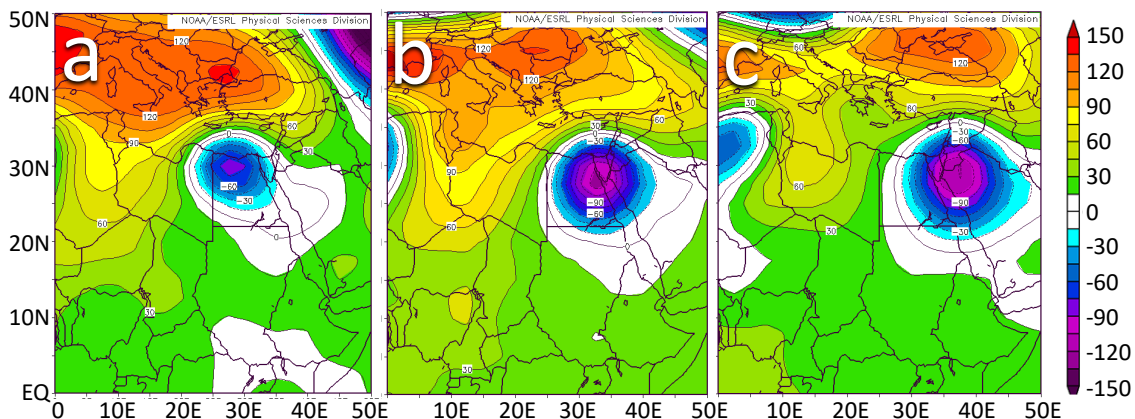
175

Figure 6: GPH anomaly at 500 hPa in 12 UTC for 24–26 April 2018, a–c, respectively. Panels a and b demonstrate the split of a large anticyclone, covering Europe, into two vortices. The eastern one, together with the cyclone over the south-eastern Mediterranean, form the dipole described in the text. Arrows in c show the induced flow of each of the two vortices.
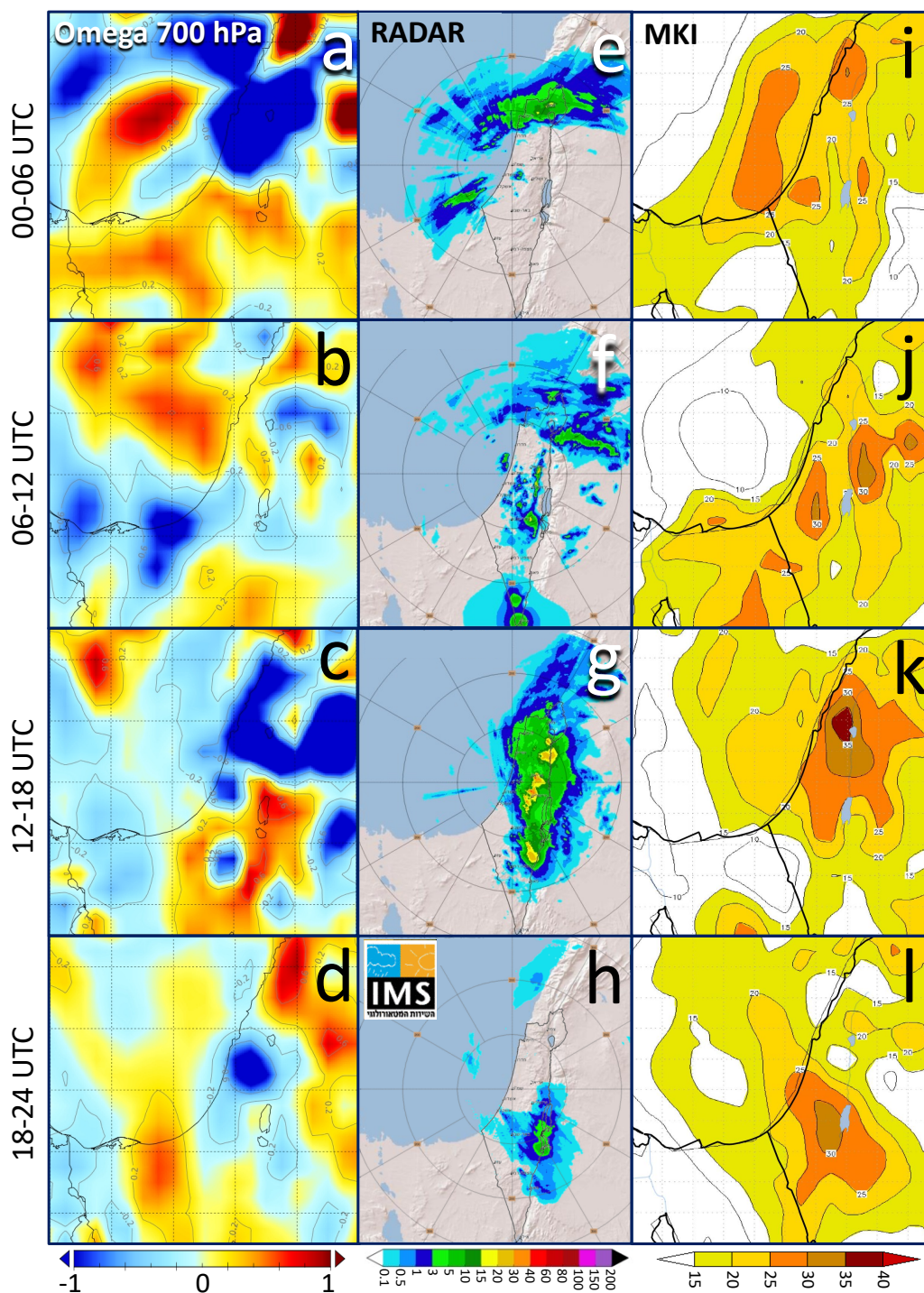
180 **Figure 7: 700 hPa vertical velocity (Omega, in Pascal s⁻¹ units, negative values in blue - reflect ascending motion) for 03, 09, 15 and 21 UTC (a–d, respectively); Radar imagery of integrated rain depth (mm) at 6 hour intervals for 00–06, 06–12, 12–18 and 18–24 UTC (e–h, respectively); and MKI for 03, 09, 15 and 21 UTC (i–l, respectively).**

3.2 Dynamic conditions

Figure 7 demonstrates the association between the dynamic factor (and the thermodynamic factor, as described in Sec. 3.3),
185 represented by the 700 hPa Omega, at a meso-scale resolution of 0.25   , and the distribution of the rain systems, as detected
by the radar. In the morning of April 26, the most prominent feature is a zonally oriented cloud strip, extending over western
Syria and north Israel (Figs. 7e and 7f). This strip was co-located with a region of negative Omega (ascendance of >10 Pa s^{-1},
Figs. 7a and b), implying that this rain system is supported by the dynamic factor.

Toward noon time, this cloud system rotated cyclonically and became meridionally oriented, as can be inferred from both the
190 radar imagery and the ascending area (Figs. 7g and 7c, respectively), which was parallel to the mountain ridges of Israel (Fig.
1). Three rain centers are noted within this system (Fig. 7g): one, the northernmost, was located at the Jordan valley, the central,
spread along the mountains' upslope, and hence can be considered as forced by orography, and the southernmost, which caused
the fatal flood, over a relatively flat terrain (denoted Tzafit in Fig. 1). It should be noted that the three rain centres are located
within a region of negative Omega (ascendance, Fig. 7c), with an extremum value of ~ -10 Pa s^{-1}. This implies that these rain
195 systems are dynamically supported. In the late afternoon, southern Israel was still under precipitative cloudiness (Fig. 7h), but
the dynamic signature, i.e., the vertical ascent dropped to ~ -0.1 Pa s^{-1} there (Fig. 7d).

The characteristics of the upper-level cyclone in this event were extreme for the pertinent season. An objective 500 hPa cyclone
climatology for the Mediterranean region for 45 years by Campins et al., (2011) points at cyclone radii between 350 and 700
km. The radii of the 500 hPa cyclones for the 28 days in the reference period (defined in Sec. 2) vary between 275 and 1170
200 Km, with an average of 625 km (Table 1). On the day of the flood (April 26), the radius of the upper-level cyclone was the
smallest, 275 km, while located over Jordan (Fig. 3c). The effect of the small radius of the upper-level cyclone can be estimated
by a measure of its curvature vorticity (MCV). A comparison of all the 28 days (Table 1) indicates that for the storm analysed
here the MCV is the highest of them all.

205 **Table 1.** Measure of curvature vorticity, depth and radius of the 500 hPa cyclones for the days in April–May during the period
1986–2018, in which discharge was recorded over the study area.

Date	Depth (m)	Radius (Km)	MCV (s$^{-1}\times10^5$)
1986/04/02	60	385	5.5
1986/04/03	15	720	0.4
1986/04/08	45	630	1.5
1986/04/09	15	1170	0.1
1997/05/14	15	688	0.4
2001/04/04	105	440	7.4
2001/04/05	15	375	1.5
2001/04/30	15	440	1.1
2001/05/01	30	450	2.0

2001/05/02	90	1170	0.9
2001/05/03	75	720	2.0
2007/05/12	45	540	2.1
2011/04/04	45	810	0.9
2011/04/05	15	1080	0.2
2014/05/07	30	540	1.4
2014/05/08	60	275	10.8
2014/05/11	30	900	0.5
2014/05/12	15	630	0.5
2015/04/16	30	810	0.6
2016/04/10	60	813	1.2
2016/04/11	60	330	7.5
2016/04/12	30	1000	0.4
2016/04/13	45	500	2.5
2016/04/14	45	750	1.1
2018/04/24	60	330	7.5
2018/04/25	90	330	11.2
2018/04/26	75	275	13.5
2018/04/27	60	385	5.5

3.3 Thermo-dynamic conditions

210 During the approach of the upper-level cyclone, the thermodynamic state of the atmosphere over the study region became more and more favourable for convection. Figure 3 shows the values of leading instability indices, specified in Sec. 2, derived from Beit Dagan soundings, in 24-hour increments. They reflect a gradual increase toward April 25 12 UTC, while the upper-level cyclone approached the Sinai Peninsula. At that time, the values of CAPE (779 J Kg^{-1}), LI (-4.9 K) and SI (-2.7 K) indicate potential for thunderstorms. At the same time, the precipitable water over the study area, increased from 17 mm, while

215 the upper-level cyclone approached the western tip of the Nile delta, to 30 mm in April 25 12 UTC. During April 26, the moisture content remained between 26 and 27 mm, while the CAPE rose to 909 J Kg^{-1}. The sharp increase in the precipitable water can be explained by the wind shift to the northwest direction in the lower levels, which induced onshore flow throughout the troposphere (Fig. 2). The MKI distribution over the study region for the April 26, at 03, 09, 15 and 21 UTC, is shown in Figs. 7i–l, respectively. Values exceeding 25ºC, indicating potential for thunderstorms, are co-located with the major rain

220 centres at the hours 09, 15 and 21 UTC.
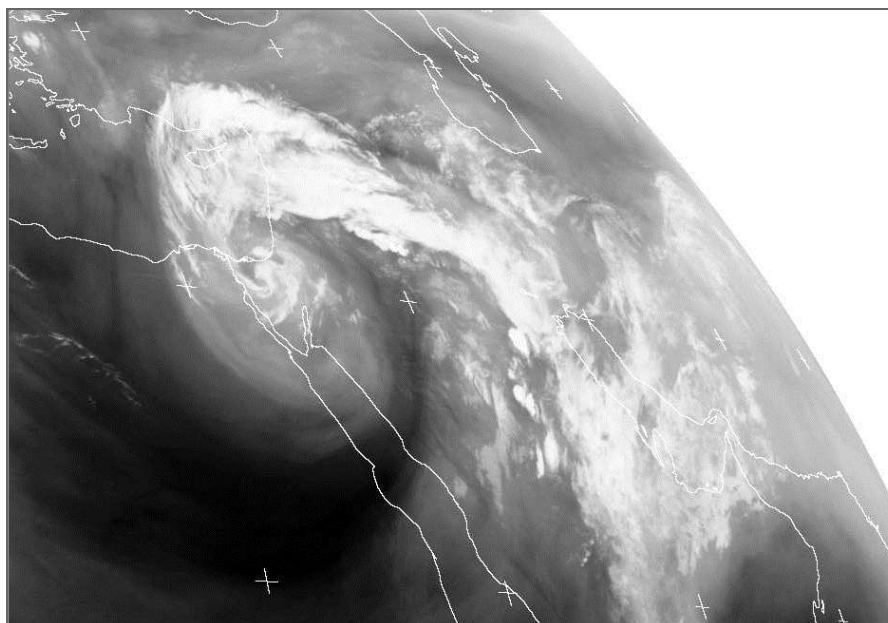
Figure 8: Water Vapor channel 6 (6.85–7.85 μm) imagery of METEOSAT from 25 April 2018 21 UTC showing the cloud strip entering Israel from the east and the vortex over the south-eastern Mediterranean (from: http://www.sat.dundee.ac.uk/xrit/000.0E/MSG/2018/4/26/300/2018_4_26_300_MSG4_5_S1_grid.jpeg).

225 The moisture transport is noted in the satellite imagery of the water vapor channel for April 25 21 UTC (Fig. 8). The major feature is a moisture strip that extended from tropical latitudes to Saudi Arabia, curved cyclonically through Iraq, where it interacted with deep moist convection, and entered northern Israel from the east in the morning of April 26 (Fig. 7e). The moisture of this strip seems to be the core of the cloud systems that later on, entered central and south Israel through the eastern Mediterranean (Fig. 7f), including the rain system that reached Tzafit at the noon hours (Fig. 7g). The trajectory arriving at

230 Tzafit at 1400 m (Fig. 9) was located over this convective region 18–24 hours prior the flood. The passage of the air over the Mediterranean Sea contributed further moisture to this rain system via the north-westerly winds at the lower levels, as can be inferred from the two lower trajectories shown in Fig. 9. Three moisture sources were responsible for the effectiveness of this rainstorm. One is of tropical nature, originated from East Africa, which were transported at the upper levels. The second, originated from the Fertile Crescent (western Iraq), via deep moist convection and the third is at the lower levels, from the

235 Mediterranean Sea by the north westerlies. The combined moisture, in addition to its direct effect, enhanced the instability described above.

Natural Hazards
and Earth System
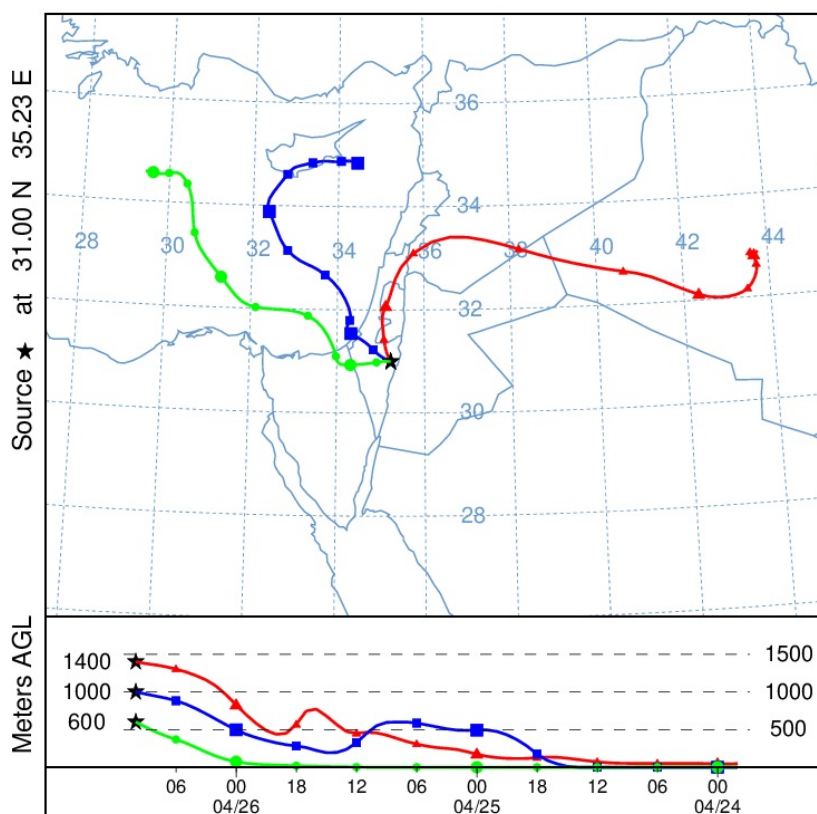
Figure 9: Sixty hours back-trajectory of the air arriving at Tzafit Creek at 26 April 2018 10 UTC at the heights 600, 1000 and 1400 m.

4 Summary and Discussion

An intense rainstorm hit the Middle East between 24 and 27 April 2018, and reached its maximum intensity on April 26, when it produced a heavy flash flood that took the lives of ten people. The study concentrates on the Negev and the Judean deserts, Israel. The rainfall observed in the southern Negev was comparable to the long-term annual rainfall (<100 mm, IMS) there. The timing of the storm is also unique, being at the end of the rainy season, when rain is relatively rare and spotty (Dayan and Sharon, 1980). The location of the surface cyclone was similar to the 'Syrian low', defined by Kahana et al. (2002) as one of the major systems causing floods in the Negev Desert.

The study analyses the dynamic and thermodynamic conditions that made this rainstorm one of the latest spring severe events in the region during the last 3 decades. The dynamic factors addressed to quantify the severity of the event are vertical velocity and curvature vorticity. The stability was estimated by (a) standard indices (LI, SI and CAPE), derived from sounding in middle Israel and (b) the Modified K index (MKI, Harats et al 2010; Ziv et al 2016) that was mapped over the region. The moisture was estimated by the vertically integrated precipitable water.

Three major rain centres were active during April 26 (Fig. 7g). One developed upslope the mountains, i.e., orographic, another in the Jordan valley and the third, which caused the fatal flood, over a relatively flat terrain. The distribution of the precipitating systems implies that synoptic and sub-synoptic atmospheric processes acted in concert. To resolve these scales, atmospheric
255 data of various resolutions were used. The mesoscale distribution of Omega and MKI confirms that the three precipitating systems were co-located with upward motion, and a maximum in the MKI.

The dynamic background of the storm was an upper-level cut-off low, with a PV maximum >1.1 PVU in the 300 hPa level (Fig. 4), typifying mid-latitude cyclones (Campa and Wernli 2012). This cyclone entered the Levant from the west along the North African coast, which is rather exceptional for late spring and the latitude along which the system moved. While
260 approaching the Levant, this upper-level cyclone slowed its movement from typical extra-tropical cyclones of ~10 ms^{-1} (Laurencin and Misra 2019) to less than 5 ms^{-1}. On the day of the flood (April 26), the radius of this cyclone was the smallest, 275 km. The effect of the small radius of this cyclone was estimated by the measure of its curvature vorticity (MCV). A comparison of all 28 days in which floods were observed over the study area during the latest 33 years (Table 1) indicates that during this storm the radius was the smallest and the MCV was the highest of them all.

265 The lower levels were dominated by a cyclone, centred east of Israel (Fig. 2). The implied winds were north-westerly, hence advecting moist air from the Mediterranean inland. During the approach of the upper-level cyclone, the atmosphere over the study region became favourable for convection. The instability indices reached values indicating potential for thunderstorms (CAPE = 909 J Kg^{-1}, LI = - 4.9 K, SI = - 2.7 K and MKI = 30 K). At the same time, the precipitable water over the study area increased from 17 to 30 mm.

270 In addition to the lower-level moisture advection, a mid-level band of tropical moisture, extending through Saudi Arabia, curved cyclonically through Iraq, gained further moisture through deep convection, and entered north Israel in the morning of April 26 from the east. At noon hours this moist air band turned left (south and then southeast) over the lower-level Mediterranean moist air. The combination of both moisture contributions can explain the high precipitable water observed over the study region. The severe rain showers over Israel are attributed directly to the moisture contribution, and indirectly,
275 to the activation of the pre-existing conditional instability.

The severity of this rainstorm can be explained by several factors:

• The small radius of the upper-level cyclone, and its resulting large curvature vorticity. The latter, approximated by the MCV, was the largest among the 33-year data record (Table 1).

• The latitude along which the upper-level cyclone moved, i.e., 30   N. This is rather south of the common track of upper-level
280 cut-off lows that affect the Mediterranean (e.g., Ziv et al. 2010). This reflects the extremely high amplitude of the upper-level associated disturbance.

• The slow movement of the upper-level cyclone while crossing the region. Slow propagation of upper-level disturbances is expected to further enhance their induced dynamic effects, i.e., divergence and vertical ascent (Palmen and Newton 1969; Ziv and Paldor 1999).

285 • High static instability. The CAPE values reached 1000 J K g^{-1}. The origin of the instability is discussed below.

• Combined contribution of several moisture sources. An airstream of tropical origin was enriched by moist convection. This air merged with underneath Mediterranean moist air mass. The role that tropical moisture plays in Mediterranean rain systems has been raised by Krichak et al. (2007). A contribution of moisture from tropical latitudes was shown for a rainstorm over Israel in 6 April 2006 (Morin et al. 2007, Fig. 3).

290 • The involvement of Sub-synoptic features. On top of the synoptic-scale factors, meso-scale features were found to activate the main rain producing systems. The dominant lower-level cyclone during the storm resembles that of the 'deep cyclone to the east', which is one of the types of Cyprus lows defined by Alpert et al. (2004). Saaroni et al. (2010) showed that most of the rain associated with this type of low is obtained over the western slopes of the Judean Mountains. The existence of two out of the three non-orographic rain-producing systems emphasizes the sub-synoptic contribution.

295 An interesting point relates to the build-up of static instability under the influence of low to the east in the spring. The lower-level conditions were similar to the rainy phase of a Cyprus low. In the winter, cold air from south Europe interacts with the underneath warmer Mediterranean water and becomes unstable before entering Israel (Shay-El and Alpert 1991, Saaroni et al. 2010). In the late spring, Europe becomes warmer and the Mediterranean remains cool, so that instability is unexpected under the above conditions. In the case analysed here, the instability can be attributed to a -5 K temperature anomaly over the region,

300 caused by a northerly flow east of the blocking high that transported cold air from North Europe (see Fig. 6, above). This negative anomaly enabled the build-up of the observed instability.

4 Conclusions

The unique intensity of this storm can be attributed to an amplification of a mid-latitude disturbance, which produced a cut-off low, with high relative vorticity, low upper-level temperatures and slow progression. All these, combined with the

305 contribution of several moisture sources, led to extreme dynamic and thermodynamic conditions favourable for this exceptionally severe rainstorm. The severity of this rainstorm, and the casualties it caused, together with previous studies of similar rainstorms (some are quoted above), raise several conclusions, in particular for the EM region:

• The late spring, though denoting the end of the rainy season, still bears the potential of mid-latitude synoptic-scale intense disturbances, which can produce heavy rainstorms. This is especially true whenever such an upper disturbance turns into a cut-

310 off low.

• The combination of a cut-off low with small radius and large hypsometric depth, implies high curvature relative vorticity, with strong dynamical forcing on rain formation.

• Quasi-stationary upper level systems allow moisture accumulation causing the increase in precipitation amounts from one day to the next.

315 • Moisture originating from tropical sources during such rainstorms enriches the mid- atmospheric levels, which makes the rain formation less sensitive to availability of moisture in lower levels. Hence rain cells are expected not only over mountain upslopes, but also over low terrains such as the one that caused the deadly flood in Tzafit creek.

• The analyses of meteorological fields, in particular those attributed to meso-scale phenomena, are crucial to identify centres where torrential rains are expected. This makes regional models a central tool for short term prediction of floods and flash
320 floods.

• Despite the universality of stability indices developed to illustrate the potential for convection, few of them require adjustments and modifications to fit the area being analysed. In this study, the modified KI version adopted for the eastern Mediterranean region, has shown to be a reliable predictor for convective rain centres and therefore a good precursor for floods.

325 *Acknowledgements*:

The authors thank Noam Halfon from the IMS for the rain map, Yoav Levi from the IMS for the RADAR images, and Efrat Morin from HUJI for the hydrometric data. BZ thanks the Israeli Science Foundation (ISF, grant number 1123/17).

References

Alpert, P., Osetinsky, I., Ziv, B., and Shafir, H.: Semi-objective classification for daily synoptic systems, Application to the
330 Eastern Mediterranean climate change, Int. J. Clim., 24, 1001-1011, DOI: 10.1002/joc.1036, 2004.

Ashbel, D.: Great floods in Sinai Peninsula, Palestine, Syria and the Syrian desert, and the influence of the Red Sea on their formation. Quart. J. R. Met. Soc. 64: 635 – 639, 1938.

Aref, H.: Integrable, chaotic, and turbulent vortex motion in two-dimensional flows. A. Rev. Fluid Mech. 15, 345-389, 1983.

Becker, J.S., Taylor, H.L., Doody, B.J., Wright, K.C., Gruntfest, E., and Webber, D.: A review of people's behavior in and
335 around floodwater. Weat., Clim. Soc. 7, 321–332, DOI: 10.1175/WCAS-D-14-00030.1, 2015.

Campa, J., and Wernli, H.: A PV Perspective on the Vertical Structure of Mature Midlatitude Cyclones in the Northern Hemisphere Article in J. Atmos. Sci. 69, 725-740, https://doi.org/10.1175/JAS-D-11-050.1, 2012.

Campins, J., Genoves, A., Picornell, M.A., and Jansa, A.: Climatology of Mediterranean cyclones using the ERA-40 dataset, Int. J. Clim., 31, 11, 1596-1614, https://doi.org/10.1002/joc.2183, 2011.

340 Copernicus Climate Change Service (C3S) (2017): ERA5: Fifth generation of ECMWF atmospheric reanalyses of the global climate. Copernicus Climate Change Service Climate Data Store (CDS), accessed: 25 December 2019. https://cds.climate.copernicus.eu/cdsapp#!/home

Dayan, U., and Morin, E. : Flash Flood-Producing rainstorms over the Dead Sea, Israel: A Review, in Enzel, Y., Agnon, A., and Stein, M., eds., New Frontiers in Dead Sea paleoenvironmental research: Geological Society of America Special Paper
345 401, doi: 10.1130/2006/2401(04), 2006.

Dayan, U. and Sharon, D.: Meteorological Parameters for Discriminating Between Widespread and Spotty Storms in the Negev. Israel Journal of Earth Sciences, 29 (4), 253-256, 1980.

Diakakis, M., Priskos, G. and Skordoulis, M.: Public perception of flood risk in flash flood prone areas of Eastern Mediterranean: the case of Attica Region in Greece. InternationalJournal of Disaster Risk Reduction, 28, 404-413,
350   https://doi.org/10.1016/j.ijdrr.2018.03.018, 2018.

Flocas, H., Maheras, A.M.P., Karacostas, T.S., Patrikas, I. and Anagnostopoulos, C.: A 40-year climatological study of relative vorticity distribution over the Mediterranean, Int. J. Climat., 21, 1759 – 1778, doi: 10.1002/joc.705, 2001.

Galateia, T., Ruin, I., Anquetin, S., and Gourley, J.J.: A situation-based analysis of flash flood fatalities in the united states, B. Am. Meteorol. Soc., 333-345, https://doi.org/10.1175/BAMS-D-15-00276.1, 2017.

355   Galway, J. G.: The lifted index as a predictor of latent instability, B. Am. Meteorol. Soc., 37, 10, 528-529, 1956.

Geer, I. W.: Glossary of Weather and Climate, Am. Meteorol. Soc., 131, 1996.

Greenbaum, N., Schwartz, U., and Bergman, L.: Extreme floods and short-term hydroclimatological fluctuations in the hyper-arid Dead Sea region, Israel, Global and Planetary Change, 70, 1–4, 125-137, 2010, https://doi.org/10.1016/j.gloplacha.2009.11.013, 2010.

360   Harats, N., Ziv, B., Yair, Y., Kotroni, V., and Dayan, U,: Dynamic and thermodynamic predictors for lightning and flash floods in the Mediterranean, Adv. Geophys., 23, 57-64, 2010

HMSO 1962. Weather in the Mediterranean I: General Meteorology. 2nd edn. Her Majesty's Stationery Office: London, 362.

Hoskins, B. J., McIntyre, M.E., and Robertson, A.W.: On the use and significance of isentropic potential vorticity maps, Q. J. Roy. Meteo. Soc., 877-946, https://doi.org/10.1002/qj.49711147002, 1985.

365   Jacobeit, J., Homann, M., Philipp, A., and Beck, C.: Atmospheric circulation types and extreme areal precipitation in southern central Europe. Advances in Science and Research 14: 71-75, 2017.

Kahana, R., Ziv, B., Enzel, Y. and Dayan, U.: Synoptic climatology of major floods in the Negev Desert, Israel. Int. J. Climat. 22, 867-882, https://doi.org/10.1002/joc.766, 2002.

Kalnay, E., Kanamitsu, M., Kistler, R., Collins, W., Deaven, D., Gandin, L., Iredell, M., Saha, S., White, G., Woollen, J., Zhu,
370   Y., Chelliah, M., Ebisuzaki, W., Higgins, W., Janowiak, J., Mo, K. C., Ropelewski, C., Wang, J., Leetmaa, A., Reynolds, R., Jenne, R., and Joseph, D: The NCEP/NCAR 40-years reanalysis project, B. Am. Meteorol. Soc., 77, 437–472, https://ui.adsabs.harvard.edu/link_gateway/1996BAMS...77..437K/doi:10.1175/1520-0477(1996)077%3C0437:TNYRP%3E2.0.CO;2,1996.

Kistler, R., Kalnay, E., Collins, W., Saha, S., White, G., Woollen, J., Chelliah, M., Ebisuzaki, W., Kanamitsu, M., Kousky,
375   V., Van Den Dool, H., Jenne, R., and Fiorino, M: The NCEP-NCAR 50-year Reanalysis: Monthly means CD-ROM and documentation, B. Am. Meteorol. Soc., 82, 247–267, doi:10.1175/1520-0477(2001)082<0247:TNNYRM>2.3.CO;2, 2001.

Knippertz, P., Pantillon, F., and Fink, A.H.: The devil in the detail of storms, Environ. Res. Lett. 13 (2018) 051001, https://doi.org/10.1088/1748-9326/aabd3e, 2018.

Kossin, J. P.: A global slowdown of tropical-cyclone translation speed, Nature 558, 104–107, doi:10.1038/s41586-018-0158-
380   3, 2018.

Krichak, S.O., Alpert, P., and Dayan, M.: An evaluation of the role of hurricane Olga (2001) in an extreme rainy event in Israel using dynamic tropopause maps. Meteor Atmos Physics, 98, 1-2, 35-53, DOI 10.1007/s00703-006-0230-7, 2007.

Laurencin, C.N. and Misra, V.: Characterizing the variations of the motion of the North Atlantic tropical cyclones, Meteorol. Atmos. Phys.131,2,225-236. https://doi.org/10.1007/s00703-017-0566-1, 2019.

385 Lionello, P., Dalan, F., Elvini, E.: Cyclones in the Mediterranean region: the present and the doubled CO2 climate scenarios. Clim Res 22:147–159, 2002.

Liu, W. T.: Statistical relation between monthly mean precipitable water and surface-level humidity over global oceans, Mon. Weather Rev, 114, 1591-1602, http://dx.doi.org/10.1175/1520-0493(1986)114<1591:SRBMMP>2.0.CO;2, 1986.

Marra, F., and Morin, E.: Use of radar QPE for the derivation of Intensity–Duration–Frequency curves in a range of climatic

390 regimes, Journal of Hydrology 531, 427–440. http://dx.doi.org/10.1016/j.jhydrol.2015.08.064, 2015.

Moncrieff, M.W. and Miller, M., J.: The dynamics and simulation of tropical cumulonimbus and squall lines, Quart. J. R. Met. Soc. (1976), 102, 373-394, 1976.

Montz, B.E., Gruntfest, E.: Flash flood mitigation: Recommendations for research and applications. Global Environmental Change Part B: Environmental Hazards, 4(1), 15–22, https://doi.org/10.1016/S1464-2867(02)00011-6, 2002.

395 Morin, E., Harats, N., Jacoby, Y., Arbel, S., Getker, M., Arazi, A., Grodek, T., Ziv, B., and Dayan, U.: Studying the extremes: hydrometeorological investigation of a flood-causing rainstorm over Israel, Adv. Geosci., 12, 107–114, https://doi.org/10.5194/adgeo-12-107-2007, 2007.

Palmen, E. and Newton, C.W. (Eds.): Atmospheric Circulation Systems. Academic Press, New York, 1969.

Porat, A, Halfon, N and Forshpan A.: Examining the exceptionality of 25-27 April 2018, IMS August (in Hebrew), 2018.

400 Raible, C.C, Yoshimori, M., Stocker, T.F., and Casty, C.: Extreme midlatitude cyclones and their implications to precipitation and wind speed extremes in simulations of the maunder minimum versus present day conditions. Clim Dyn 28:409–423, 2007.

Saaroni, H., Halfon, N., Ziv. B., Alpert, P., and Kutiel, H.: Links between the rainfall regime in Israel and location and intensity of Cyprus lows, Int. J. Climat., 30, 1014-1025, DOI: 10.1002/joc.1912, 2010.

Sharif, H., Jackson, T., Hossain, M., and Zane, D.: Analysis of flood fatalities in Texas. Nat. Hazards Rev. 16, 04014016, DOI:

405 10.1061/(ASCE)NH.1527-6996.0000145, 2015.

Shay-El, Y., and Alpert, P.: A diagnostic study of winter diabatic heating in the Mediterranean in relation to cyclones, Quarterly Journal of the Royal Meteorological Society 117, 715–747, https://doi.org/10.1002/qj.49711750004, 1991.

Showalter, A., K.: A Stability Index for Thunderstorm Forecasting. Bull. Amer. Meteor. Soc., 34, 25-252, 1953.

Stein, A.F., Draxler, R.R, Rolph, G.D., Stunder, B.J.B., Cohen, M.D., and Ngan, F.: NOAA's HYSPLIT atmospheric transport

410 and dispersion modeling system, Bull. Amer. Meteor. Soc., 96, 2059-2077, http://dx.doi.org/10.1175/BAMS-D-14-00110.1, 2015.

Terti, G., Ruin, I., Gourley, J.J., Kirstetter, P., Flamig, Z., Blanchet, J., Arthur, A. and Anquetin, S.,: Toward probabilistic prediction of flash flood human impacts. Risk Analysis, 39, 140-161, doi: 10.1111/risa.12921, 2019.

Ulbrich, U., Leckebusch, G.C. and Pinto, J.G.: Extra-tropical cyclones in the present and future climate: a review. Theor. Appl.

415 Climatol. 96, 117–131 (2009). https://doi.org/10.1007/s00704-008-0083-8, 2009.

Wei, M., Pasquero, C., and Primeau, F.: The effect of translation speed upon the intensity of tropical cyclones over the tropical ocean, Geophysical Research Letters, 39, L07801, doi:10.1029/2011GL050765, 2012.

Yamazaki, A., and Itoh, H.: Vortex-vortex interactions for the maintenance of blocking: Part I: The selective absorption mechanism and a case study, Journal of the Atmospheric Sciences, 70, 725-742, DOI: 10.1175/JAS-D-11-0295.1, 2013.

420 Zappa, G., Hawcroft, M.K., Shaffrey. L., Black, E., and Brayshaw, O.J.: Extratropical cyclones and the projected decline of winter Mediterranean precipitation in the CMIP5 models, Climate Dynamics, doi: I 0. 1007/s00382-0 14-2426-8, 2015.

Ziv, B., Dayan, U., Kushnir, Y., Roth, C., and Enzel, Y.: Regional and global atmospheric patterns governing rainfall in the southern Levant, Int. J. Climat., 26, 55-73, https://doi.org/10.1002/joc.1238, 2006.

Ziv, B., Harats, N., Morin, E. et al. Can severe rain events over the Mediterranean region be detected through simple numerical

425 indices? Nat Hazards 83, 1197–1212, 2016.

Ziv, B., and Paldor, N.: The Divergence field associated with time dependent jet streams, J. Atmos. Sci., 56 No. 12, 1843-1857, 1999.

Ziv, B., Saaroni, H., Romem, M., Heifetz, E., Harnik, N., and Baharad, A.: Analysis of conveyor belts in winter Mediterranean cyclones, Theor. App. Clim., 99, 3-4, 441 – 455, 2010.